A Giant Impact Origin of Pluto-Charon

Robin M. Canup

Pluto and its moon, Charon, are the most prominent members of the Kuiper belt, and their existence holds clues to outer solar system formation processes. Here, hydrodynamic simulations are used to demonstrate that the formation of Pluto-Charon by means of a large collision is quite plausible. I show that such an impact probably produced an intact Charon, although it is possible that a disk of material orbited Pluto from which Charon later accumulated. These findings suggest that collisions between 1000-kilometer-class objects occurred in the early inner Kuiper belt.

The Pluto-Charon pair shares key traits with the Earth-Moon system. Each satellite mass is substantial compared to its planet: Charon's mass is 10 to 15% of Pluto's mass, and the Moon's mass is ~1% of Earth's mass. All other satellite-to-planet mass ratios in our solar system are less than $\sim 2 \times 10^{-4}$. The orbits of Charon and the Moon are consistent with a scenario in which each satellite formed much closer to its planet, and torques due to tides raised on the planet by the satellite subsequently caused the satellite's orbit to expand to its current separation. The angular momentum of both pairs is large, within a factor of several of the critical angular momentum for rotational stability of a single object containing the total system mass.

In both cases, an origin by "giant impact," in which a large oblique collision with the growing planet produced its satellite and provided the system with its angular momentum, is favored (1–4). However, to date, the viability of this mode of origin has only been demonstrated for the Earth-Moon case. Models of lunar-forming impacts (4–7) produce disks orbiting the planet containing about 1 to 3% of the planet's mass, and as such the feasibility of forming the proportionally more massive Charon has been unknown. Although giant impacts are believed common in the final stage of terrestrial planet formation in the inner solar system (8), their role in the outer solar system and the Kuiper belt [a disk of objects orbiting exterior to Neptune between about 30 and 50 astronomical units (AU)] is more uncertain (9). The origin of Pluto-Charon provides a key constraint to this issue and to the population of objects in the primordial Kuiper belt.

Properties of the distant Pluto-Charon pair [supporting online material (SOM)

Southwest Research Institute, Boulder, CO 80302, USA, and Division of Geological and Planetary Sciences, California Institute of Technology, Pasadena, CA 91125, USA. E-mail: robin@boulder.swri.edu

text] remain somewhat uncertain. Pluto and Charon have physical radii of $R_P \approx 1150$ to 1200 km and $R_C \approx 590$ to 620 km, and their densities are $\rho_P \approx 1.8$ to 2.1 g/cm^3 and $\rho_C \approx 1.6$ to 1.8 g/cm^3, indicating rock-ice compositions with about 50 to 80% rock by mass (10). Scaling the angular momentum of the Pluto-Charon binary, L_{PC}, by the quantity $L' \equiv \sqrt{GM_{PC}^3 R_{PC}}$ (where R_{PC} is the radius of an equivalent spherical object containing the total Pluto-Charon system mass, M_{PC}, and G is the gravitational constant) gives the normalized system angular momentum, $J_{PC} \equiv L_{PC}/L'$, which is in the range $0.33 < J_{PC} < 0.46$ for a Charon-to-Pluto mass ratio, q, in the range $0.1 < q < 0.15$.

Here, I present smooth particle hydrodynamic (SPH) simulations to show that giant impacts can produce Pluto-Charon–type systems with $q > 0.1$ and $J \sim 0.4$. In SPH, an object is described by a multitude of overlapping particles, each of which represent a three-dimensional (3D) distribution of matter of a specified composition, whose properties are tracked in time in a Lagrangian manner. In these simulations, particles are evolved due to gravity, compressional heating and expansional cooling, and shock dissipation (11), and the Analytic Equation of State, M-ANEOS (12, 13), is used with material constants by Pierazzo and Melosh (14). For a full description of the SPH technique, see (15), from whose work the code used here is directly descended.

The SPH simulations involved between $N = 2 \times 10^4$ and 1.2×10^5 particles and a simulated time of 1 to 4 days. Given that the appropriate differentiation state and composition of the colliding objects is uncertain, I considered three initial compositions: (i) SER: 100% undifferentiated serpentine [Mg$_3$Si$_2$O$_5$(OH)$_4$, a hydrated silicate containing $\approx$14% H$_2$O by weight]; (ii) IDI: 40% water ice, 42% dunite, and 18% iron by mass and differentiated into

an ice mantle, rock core, and iron inner core; and (iii) SIM: 50% serpentine and 50% water ice in an undifferentiated mixture. These objects range from uniform to highly differentiated, with rock mass fractions between 43 and 86% and bulk densities between ~1.5 to 2.5 g/cm^3.

I modeled a variety of impacts that were all capable of providing an angular momentum within the range for Pluto-Charon. The collision of two nonspinning equal density objects delivers a normalized angular momentum (16)

$$J_{col} \equiv \frac{L_{col}}{L'} = \sqrt{2} f(\gamma) b' \left(\frac{v_{imp}}{v_{esc}} \right) \quad (1)$$

where $b' \equiv \sin \xi$ is the scaled impact parameter, ξ is the angle between the surface normal and the impact trajectory (a grazing impact has $b' = 1$), γ is the impactor-to-total mass ratio, $f(\gamma) \equiv \gamma(1 - \gamma)\sqrt{\gamma^{1/3} + (1 - \gamma)^{1/3}}$, and (v_{imp}/v_{esc}) is the ratio of the impact velocity to the mutual escape velocity, with $v_{imp}^2 \equiv v_{esc}^2 + v_\infty^2$, where v_∞ is the relative velocity at large separation. Here, $v_{esc} \equiv \sqrt{2GM_T/(R_{imp} + R_{tar})}$, where M_T is the total colliding mass, and R_{imp} and R_{tar} are the impactor and target radii, respectively. A preimpact spin [due to earlier impacts (8, 17)] that had a component in the same rotational sense as the impact ("prograde") would increase J_{imp}. For the case of prograde spin vectors normal to the plane of the impact, the additional contribution is

$$J_{spin} = K_{imp} \frac{T_{min}}{T_{imp}} \gamma^{5/3} + K_{tar} \frac{T_{min}}{T_{tar}} (1 - \gamma)^{5/3} \quad (2)$$

where $J_{imp} = J_{col} + J_{spin}$, K_{imp} and K_{tar} are the moment of inertia constants of the colliding objects, T_{imp} and T_{tar} are the preimpact spin periods of the impactor and target, and the minimum period for rotational stability is $T_{min} \equiv \sqrt{3\pi/(G\rho)} = 2.3$ hours $(\rho/2g/cm^3)^{-1/2}$, where ρ is the density of the objects. Here, collisions with $0.5 < b' < 1$, $1 < (v_{imp}/v_{esc}) < 2.5$ (or $0 < v_\infty < 2.5$ km/s), $0.13 < \gamma < 0.5$, and with (18) and without preimpact spin are simulated.

Results. An impact between predifferentiated (IDI composition) identical objects, each of which contained 0.53 M_{PC} (so that $\gamma = 0.5$) and had an initial prograde 7-hour day, produces a planet-disk system (Fig. 1). This $b' = 0.83$ collision had $v_{imp} = v_{esc}$ and $J_{imp} = 0.43$, of which 14% was contained in preimpact spin. The resulting disk mass (Fig. 1) is 12% of the planet's mass, and 70% of the disk has equivalent circular orbits exterior to the

Roche limit, a_R (*19*). Of the initial impact angular momentum, 7% escapes (contained in 1% of the mass), 44% is in orbiting material, and ~50% is in the final planet that forms with a spin period of 2.6 hours. The final planet-disk system has $J_f = 0.40$, where $J_f \equiv L_f/\sqrt{GM_f^3 R_f}$ is the normalized system angular momentum, with M_f the total bound mass and $R_f = (3M_f/4\pi\rho)^{1/3}$. I estimated the mass of the satellite ($M_s \equiv qM_p$) that would accumulate from the disk based on models of lunar accretion (*20*). Assuming that disk material with mass M_D and angular momentum L_D will either be accreted onto the planet of mass M_p or into a single satellite with semimajor axis $a_s \approx 1.2a_R$ (*20*, *21*)

$$M_s \approx 1.9L_D/\sqrt{GM_p a_R} - 1.1M_D \qquad (3)$$

For this case (Fig. 1), $q \approx 0.12$.

A collision involving undifferentiated SER objects, a smaller impactor ($\gamma = 0.3$), and no initial spin produces a planet-moon system (Fig. 2). A very grazing collision ($b' = 0.96$) is needed to supply sufficient angular momentum for this smaller γ and $v_{imp} = v_{esc}$. The result is a binary with $q = 0.125$, eccentricity $e = 0.50$, a 3500-km (or 3.25 R_p) periapse separation, and a normalized final angular momentum $J_f = 0.36$. The planet's rotation period is 5.2 hours, with 55% of the initial angular momentum contained in the satellite.

Table 1 and table S1 detail simulations that produced a planet-moon or planet-disk system within the plausible mass-ratio range for Pluto-Charon together with $J_{imp} \geq 0.33$. Results from 120 simulations that had $0.3 < J_{imp} < 0.6$ and $M_T \sim M_{PC}$ are shown in Fig. 3 and fig. S1. Resulting planet-moon systems had satellite semimajor axes ranging from 3.7 to 21 R_p, periapses from 2.5 to 5 R_p, and $0.1 < e < 0.8$. Intermediate outcomes to those in Fig. 3 would be expected for values between those sampled here ($0.3 < \gamma < 0.5$).

The formation of intact moons is correlated with the impactor's differentiation state, with $b' > 0.8$ collisions by undifferentiated impactors typically yielding moons on stable orbits, whereas IDI impactors with $b' > 0.8$ did not. From basic thermal arguments (*22*), an early impactor containing ~30 to 50% of Pluto's mass would likely have been undifferentiated. Compared to the disk-producing impacts, the intact moon cases surround the (q,J) region of the Pluto-Charon system much more completely (Fig. 3 and fig. S1) and produce $0.1 < q < 0.15$ satellites for $b' > 0.8$, $J_{imp} > 0.3$, and $v_{imp} \leq 1.2v_{esc}$. This greater range in J_{imp} and v_{imp} than the successful disk-producing cases (SOM text and table S1) corresponds to a greater range in the other impact variables (Eqs. 1 and 2), with successful intact moon cases occurring for $0.3 \leq \gamma \leq$ 0.5 and with or without initial spins. Given these data, the formation of an intact Charon appears the more probable mode of origin.

Whereas both massive disks and intact moons are produced by very oblique impacts ($b' > 0.8$), the moon cases typically involve a higher fractional partitioning of mass and angular momentum into orbiting material than the disk cases. This is primarily due to a difference in the nature of the gravitational torques that allow for orbital emplacement. For disk cases, impactor material is sheared into trailing spiral-arm structures (Fig. 1, D and E) (*7*), a configuration that is effective in transporting angular momentum from radially inner to outer portions. This torque causes inner arm material to accrete onto the planet, whereas the outermost material either goes into bound orbit or escapes. In the intact moon cases, the angular momentum exchange occurs primarily between the distorted figure of the target planet and a condensed region of impactor material (Fig. 2, B to E), and so in these cases the angular momentum sacrificed

to lift material into stable orbit is to a much greater degree derived from the planet, resulting in characteristically slower rotating planets and higher angular momentum and mass satellites. Intact moon formation is aided by a prograde spin of the impactor after the initial impact, which helps to counteract the shearing of impactor material due to differential Kepler motion; this can result from an initial prograde impactor or retrograde target spin, or from a highly grazing impact.

One overall implication of my simulations is that collisionally producing systems with $J \sim J_{PC}$ is correlated with the production of satellites that have $(M_s/M_p) = q \sim O(10^{-1})$. A second result is that oblique collisions with $v_{imp} \geq 1.3v_{esc}$ (or $v_\infty \geq 0.9$ km/s for $M_T \sim M_{PC}$) do not produce massive disks or satellites orbiting the primary, and this was true for all of the simulations.

The differentiation state and composition of Pluto and Charon could have been affected by a Charon-forming impact. For disk-producing cases, ice initially at temperatures $T \sim 150$ K

Fig. 1. Time series of a potential Pluto-Charon–forming impact yielding a planet-disk system (run 70 in table S1 with $N = 120,000$ particles). Results are shown looking down onto the plane of the impact at times $t = 1.3$, 3.2, 7.5, 11.8, 14.5, and 24.6 hours; units shown are distance in 10^3 km. Color indicates material type (blue, water ice; orange, dunite; red, iron), with all of the particles in the 3D simulation overplotted in order of increasing density. The impacting objects are identical—both are predifferentiated into 40% ice mantles and 60% rock cores by mass with initial surface temperatures set to 150 K, increasing with depth (*7*) to a central temperature ≈800 K. After an initially oblique impact in the counterclockwise sense (**A**), the two objects separate (**B** and **C**) before recolliding. After the second collision, the denser cores migrate toward the center, as a bar-type mode (*36*) forms in the rapidly rotating merged objects (D). From each end of the bar emanate spiral structures (**D** and **E**), whose self-gravity acts to transport angular momentum from inner to outer portions. The arms wrap up on themselves and finally disperse to yield a ring (*36*) of material (whose differential motion would on a longer time scale produce a disk), together with the central planet (**F**).
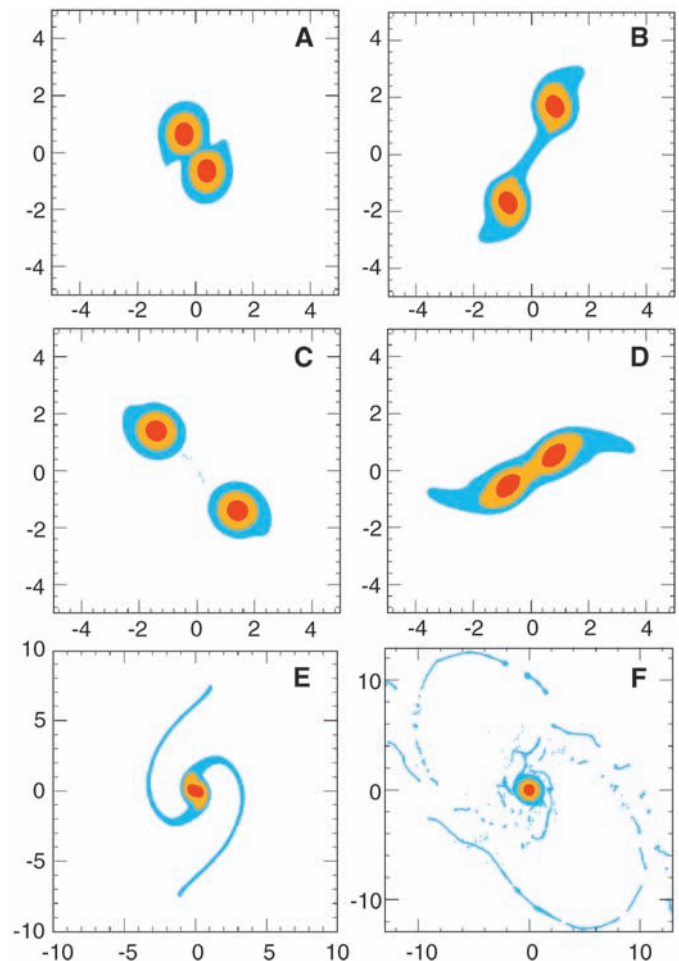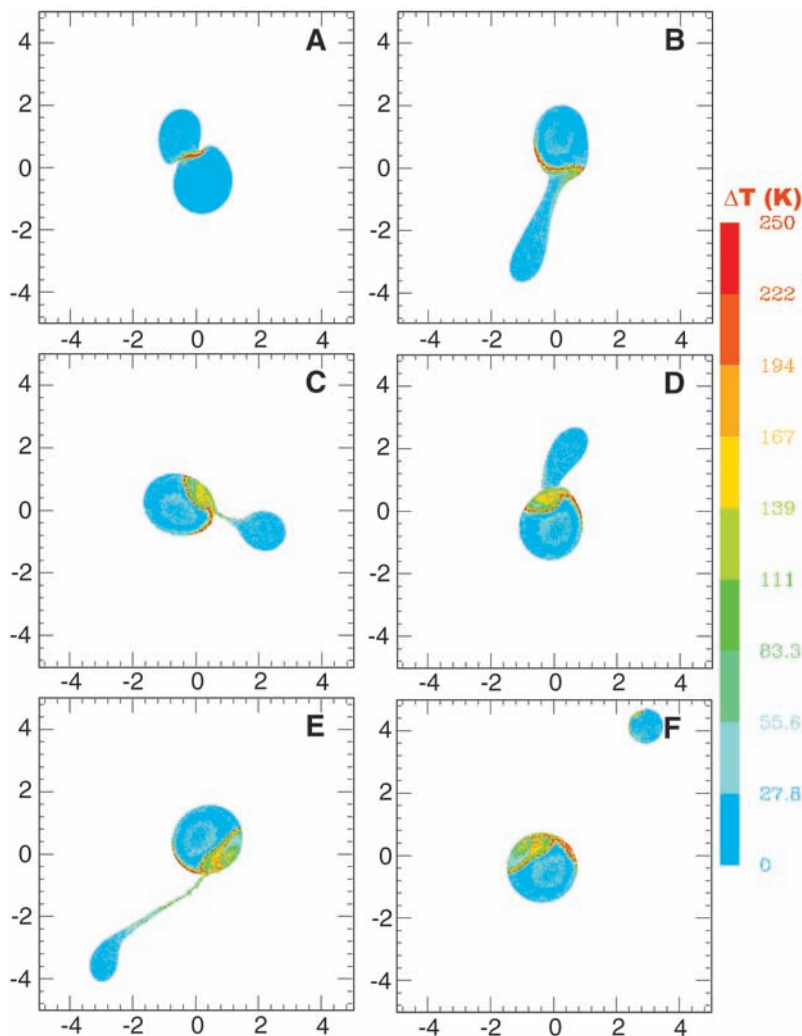
Fig. 2. Time series of a potential Pluto-Charon–forming impact yielding a planet-moon system (run 20 in Table 1 with $N = 20{,}000$ particles). Results are shown at times $t = 0.9$, 3.2, 5.9, 7.5, 11.2, and 27.5 hours; distances are shown in units of 10^3 km and color scales with the change in temperature in kelvin. The impacting objects have uniform serpentine compositions. After an initially very oblique impact with a $73°$ impact angle (**A**), the two objects separate (**B** and **C**) and during this period the smaller impactor receives a net torque from the distorted figure of the target. After a second, even more grazing encounter (**D**), an additional portion of the impactor is accreted onto the planet, while the rest self-contracts into an intact moon containing 12% of the central planet's mass that is again torqued by the ellipsoidal figure of the target (**D** and **E**) onto a stable orbit with a semimajor axis of 6.5 R_P and an eccentricity of $e = 0.5$. The final moon in (**F**) is described by 2232 SPH particles.

Table 1. Parameters and results of impacts that yield moons with $0.1 < q < 0.15$. Simulations here involved undifferentiated objects. The preimpact spin state of the objects is shown by the fraction $(L_s/L_{imp}) = (\overrightarrow{L}_s \cdot \overrightarrow{L}_{imp})/|L_{imp}^2|$; superscripts i and it correspond, respectively, to L_s contained in the impactor or the impactor and target. L_{orb} is the angular momentum of the satellite, and J_f is the normalized final bound system angular momentum.

Run	M_T/M_{PC}	γ	b'	v_{imp}/v_{esc}	J_{imp}	L_s/L_{imp}	L_{esc}/L_{imp}	M_{esc}/M_T	L_{orb}/L_{imp}	J_f	q
5	1.00	0.3	0.852	1.00	0.508	0.38[it]	0.06	0.010	0.378	0.486	0.102
6	1.00	0.3	0.785	1.00	0.483	0.40[it]	0.01	0.002	0.365	0.480	0.108
33	1.00	0.3	0.853	1.20	0.397	0.04[i]	0.00	0.000	0.514	0.397	0.115
1	1.00	0.3	0.918	1.00	0.379	0.10[i]	0.00	0.000	0.584	0.379	0.120
19	1.00	0.3	0.853	1.00	0.333	0.05[i]	0.00	0.000	0.529	0.333	0.125
20	1.00	0.3	0.957	1.00	0.356	0.00	0.00	0.000	0.545	0.356	0.125
7	1.00	0.3	0.958	1.00	0.379	0.06[i]	0.00	0.000	0.447	0.379	0.131
16	0.95	0.5	0.899	1.00	0.452	0.12[i]	0.00	0.000	0.508	0.452	0.144
21	0.95	0.5	0.862	1.05	0.454	0.11[i]	0.00	0.000	0.505	0.454	0.148
22	1.00	0.3	0.924	1.05	0.372	0.03[i]	0.00	0.000	0.588	0.372	0.149

in the region of the initial impact achieved a maximum $T \sim 300$ K ($\Delta T \sim 150$ K), with most of the ice heated to $T \sim 200$ K ($\Delta T \sim 50$ K), consistent with previous estimates (*2*). In moon-producing impacts, the satellite material experienced little heating ($\Delta T \sim 30$ K), because it had for the most part avoided direct impact with the planet, whereas the target was heated more substantially (Fig. 2).

For Pluto, the short-term heating processes associated with a large impact in combination with general accretional heating ($E_{acc}/M_P \sim 3/5[GM_P/R_P]$ could provide up to $\Delta T \sim 300$ K) and long-lived radiogenic heating ($\Delta T \leq 285$ K after 400 million years) seems most consistent with substantial melting and a differentiated state (*22*), although uncertainty associated with the rheology of rock-ice mixtures can affect this conclusion. The case for differentiation is much weaker for smaller Charon (*22*), and the results here reinforce this (*23*), particularly in the intact formation mode.

For $v_{imp}/v_{esc} \sim$ unity and $M_T \sim M_{PC}$, there is not appreciable vaporization of water ice, and successful impacts (Table 1 and table S1) lose only between 0 and 8% of their mass to escaping material. Thus, the increase in the overall rock-to-ice ratio of the pair as a result of a Charon-forming impact is expected to be modest to none. The intact moons contain material originating from the impactor with a similar bulk composition. In the collisions involving mixed compositions that produced disks, the denser components of the colliding objects migrated inward into the central planet (Fig. 1, D and E), leaving a disk of the preferentially lower density material (SOM text). Thus, if the impactor and proto-Pluto had similar overall ice-rock fractions, forming Charon from a disk implies $\rho_C < \rho_P$, whereas forming the satellite intact implies $\rho_C \sim \rho_P$. Both cases imply that the current total rock-ice fraction of the pair is similar to that of its progenitors.

Discussion. This work identifies a range of impacts capable of producing Pluto-Charon–type systems. The impacts are low-velocity ($v_\infty < 0.9$ km/s) oblique collisions by an impactor containing 30 to 50% of the Pluto-Charon system's mass, which often involve some preimpact spin of a magnitude similar to that estimated for other outer solar system bodies (*24*). The broadest range of successful impacts involves the intact formation of Charon rather than its accretion from an impact-generated disk. An intact formation implies similar planet and satellite densities, an initially eccentric satellite orbit, and characteristically larger possible satellite-to-planet mass ratios.

What is the probability of such an event? For random impact orientation (*8*), $\sim 30\%$ of collisions have $b' > 0.8$. The frequency of large impacts in the early Kuiper belt is uncertain, as the current belt is believed to contain only a small portion of its original mass

(25) and to be more dynamically excited now ($\langle v_{rel}^2\rangle^{1/2} \sim 1.5$ km/s) than when large objects formed there [$\langle v_{rel}^2\rangle^{1/2} \ll 1$ km/s (26)]. Recent accretion simulations that produce $\sim 10^3$-km Kuiper belt objects (KBOs) (26) predict a large-body cumulative size distribution $N_o(>R) \propto R^{-q'}$ with $q' \sim 3$. This implies several tens of objects as large as those considered here ($800 < R$-km < 1100) to be consistent with the formation of $\sim 10^5$ KBOs with R > 50 km as estimated from current surveys (26). A "particle-in-a-box" estimate gives the characteristic time between large impacts in the Kuiper belt region

$$\tau_{col} \approx \frac{2\pi a \Delta a H}{N_e^2 \pi (R_e + R_e)^2 v_{rel}\left[1 + \left(\frac{v_{esc}}{v_{rel}}\right)^2\right]}$$

$$\sim 10^9 \text{ years} \left(\frac{T_{orb}}{250 \text{ years}}\right)\left(\frac{50}{N_e}\right)^2$$

$$\times \left(\frac{10^3 \text{km}}{R_e}\right)^2 \left(\frac{10^2}{f}\right) \qquad (4)$$

where Δa and $H \approx v_{rel}/\Omega$ are the width and height of the disk annulus, respectively, $T_{orb} \equiv 2\pi/\Omega$ is the orbital period, $f \equiv [1 + (v_{esc}/v_{rel})^2]$ is the gravitational focusing factor, and v_{rel} is the relative velocity between large embryos of radius R_e and number N_e. In the current belt, $f \sim$ unity and large collisions occur too infrequently to be relevant.

If the early Kuiper belt contained a substantially greater number (27) of 10^3-km-class KBOs than the current belt [with such objects later lost, e.g., through dynamical scattering (28)] and/or had much lower characteristic relative velocities and strong gravitational focusing, large impacts would have been more common. In the primordial accretionary epoch, estimated velocities for $R \sim 10^3$ km objects are $v_{rel} \sim O(10^{-2}$ to $10^{-1})$ km/s (26) or $f > 10^2$ for $v_{esc} \sim 1$ km/s with $\tau_{col} < 10^9$ years. Large objects formed through so-called oligarchic growth with low v_{rel} could have become orbitally isolated from one another and thus have grown primarily through the accretion of small material (9, 26). However, it seems probable that such isolation would have been periodically overcome, as growing large bodies would have become increasingly dynamically crowded, leading to episodes of mutual collisions among "battling oligarchs" (9). Furthermore, the sweeping of Neptune's mean-motion resonances through the Kuiper belt as that planet began migrating outward (29) may have itself instigated large collisions in previously dynamically stable zones and/or acted to increase the surface density of large objects captured within resonances (3).

The low-velocity impacts that produce $q > 0.1$ have $v_\infty < 0.9$ km/s, which is consistent with a collision in the early Kuiper belt. However, the timing of a Charon-forming impact relative to the capture of Pluto-Charon into the 3:2 resonance with Neptune is uncertain. The binary could have formed first, at an orbital distance ~ 5 AU closer to the Sun than Pluto's current semimajor axis, and the pair later captured as Neptune's 3:2 migrated past them, with Pluto's $e \approx 0.25$ orbital eccentricity obtained subsequently (29, 30). If Pluto had been captured in the 3:2 before the Charon-forming impact, an appropriate v_∞ with a large nonresonant impactor might still have resulted (for example, in its current orbit, Pluto's e provides a velocity relative to circular orbits of 0.5 to 0.8 km/s at its periapse and apoapse), but such an impact would have likely dislodged Pluto from resonance (31, 32). Although recapture could occur (33), the probability of this is low if the pair had a substantial orbital eccentricity (i.e., <10% for $e > 0.15$) (34). A more promising scenario involves the collision of Pluto and an impactor both already trapped in the 3:2, as in this case, a lower relative velocity due to the difference in their forced and/or free eccentricities (32) could
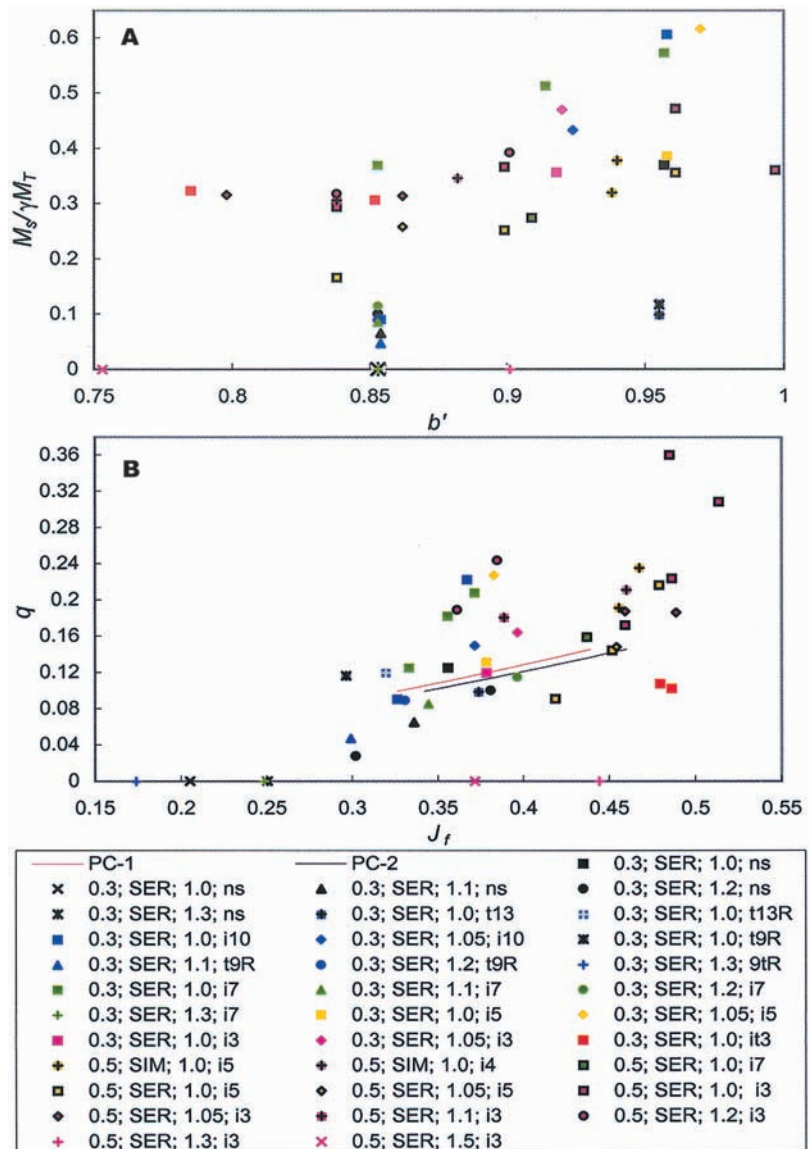

Fig. 3. Results of impact simulations that produced intact moons. Simulation parameters are shown in the legend, in which the first value is the ratio of the impactor to the total mass (γ), the second indicates the composition of the colliding objects, the third is the ratio of the impact velocity to the escape velocity, and the fourth is the preimpact prograde spin period in hours for the impactor (i) and/or target (t), with R indicating a retrograde initial spin. Cases in which an intact fragment containing 5 to 50% of the total mass escaped and little material (<1%) remained in orbit are shown as $q = 0$. (**A**) The mass fraction of the impactor that comprises the final moon versus the scaled impact parameter ($b' = 1$ for a grazing impact). (**B**) Resulting satellite-to-planet mass ratio versus the normalized angular momentum of the final bound system. In all cases, the resulting moons had periapses exterior to the co-rotation radius, $a_{co}(\sqrt{GM_T/a_{co}^3} \equiv \omega_p)$. Red and black lines bracket the parameter regime for Pluto-Charon for $0.1 < q < 0.15$ (from eq. S1).

result, and the postimpact pair might then remain in resonance.

The tendency for oblique low-velocity collisions between similarly sized objects to produce substantial amounts of material in bound orbit suggests that the impact generation of satellites is a common outcome of late-stage accretion, with the Earth-Moon ($q = 0.01$ and $J = 0.115$) and Pluto-Charon offering examples of the potential range of q and J in systems produced by such events. Requiring $(v_{imp}/v_{esc}) <$ 1.3 for forming large satellites based on the simulations here implies that binary systems produced through such singular impacts would have (from Eqs. 1 and 2) $J \lesssim 0.8$.

References and Notes

1. W. B. McKinnon, *Nature* **311**, 355 (1984).
2. W. B. McKinnon, *Astrophys. J.* **344**, L41 (1989).
3. S. A. Stern, W. B. McKinnon, J. Lunine, in *Pluto and Charon*, S. A. Stern, D. J. Tholen, Eds. (Univ. Arizona Press, Tucson, AZ, 1997), pp. 605–663.
4. R. M. Canup, *Annu. Rev. Astron. Astrophys.* **42**, 441 (2004).
5. A. G. W. Cameron, W. Benz, *Icarus* **92**, 204 (1991).
6. R. M. Canup, E. Asphaug, *Nature* **412**, 708 (2001).
7. R. M. Canup, *Icarus* **168**, 433 (2004).
8. C. B. Agnor, R. M. Canup, H. F. Levison, *Icarus* **142**, 219 (1999).
9. P. Goldreich, R. Sari, Y. Lithwick, *Annu. Rev. Astron. Astrophys.* **42**, 549 (2004).
10. C. B. Olkin, L. H. Wasserman, O. G. Franz, *Icarus* **164**, 254 (2003).
11. Our SPH simulations ignore material strength. A fluid description is valid when stresses associated with self-gravity (as well as compressional pressures associated with the impact event itself) greatly exceed the material strength, which is true for the size objects considered here (*35*).
12. H. J. Melosh, paper presented at the 31st Lunar and Planetary Science Conference, Houston, TX, 13 to 17 March 2000, abstract no. 1903.
13. S. L. Thompson, H. S. Lauson, *Sandia Natl. Lab. Technical Report No. SC-RR-710714* (Sandia Laboratories, Albuquerque, NM, 1972).
14. L. Brookshaw, Working Paper Series SC-MC-9813, Faculty of Sciences (University of Southern Queensland, Australia).
15. W. Benz, in *Proceedings of the NATO Advanced Research Workshop on The Numerical Modelling of Nonlinear Stellar Pulsations*, J. R. Buchler, Ed. (Kluwer, Boston, 1990), pp. 269–288.
16. R. M. Canup, W. R. Ward, A. G. W. Cameron, *Icarus* **150**, 288 (2001).
17. G. Tancredi, J. A. Fernandez, *Icarus* **93**, 298 (1991).
18. Rotation periods for the impactor and target between 3 and 13 hours are considered here. Estimates of rotation periods for Kuiper belt objects with $R > 10^2$ km range from about 6 (Varuna) to 14 (2001 QG298) hours (*24*).
19. The Roche limit, $a_R \equiv 2.456R_p(\rho_p/\rho_s)^{1/3}$, is the closest distance a fluid strengthless body of density ρ_s can stably exist from a radius R_p and density ρ_p primary. At the end of each run, we classified particles as escaping (positive kinetic + potential energies), orbiting, or in the planet. A particle was considered to be orbiting if its total energy was negative, and the z component of its angular momentum exceeded that of a circular orbit at the surface of the planet. We defined an equivalent circular orbit as one having the same angular momentum as computed for a given particle but with $e = 0$. If $a_{equiv} > a_R$, the particle was considered to be on a Roche exterior orbit.
20. S. Ida, R. M. Canup, G. R. Stewart, *Nature* **389**, 353 (1997).
21. The resulting satellite would be smaller if substantial mass were lost from the disk subsequent to the impact or larger if angular momentum were transferred to the disk material before the satellite formed.
22. W. B. McKinnon, D. P. Simonelli, G. Schubert, in *Pluto and Charon*, S. A. Stern, D. J. Tholen, Eds. (Univ. Arizona Press, Tucson, 1997), pp. 295–343.
23. Tides in an initially eccentric Charon-sized satellite (Fig. 2) would circularize its orbit in $\sim 10^6$ to 10^7 years (*22*), yielding $\Delta T \sim 20$ K. Rapid accretion of the satellite from a disk would produce $E_{acc}/M_C \sim 3/5[GM_C/R_C]$ or up to $\Delta T \sim 80$ K for a specific heat $C \sim 1.5 \times 10^7$ erg/g K (*33*).
24. S. S. Sheppard, D. C. Jewitt, *Astron. J.* **127**, 3023 (2004).
25. M. Holman, J. Wisdom, *Astron. J.* **105**, 1987 (1993).
26. S. J. Kenyon, *Publ. Astron. Soc. Pac.* **114**, 265 (2002).
27. S. A. Stern, *Icarus* **90**, 271 (1991).
28. J.-M. Petit, O. Mousis, *Icarus* **168**, 409 (2004).
29. R. Malhotra, *Nature* **365**, 819 (1993).
30. Pluto's current eccentricity suggests that it migrated outward by ~ 5 to 10 AU after its capture into Neptune's 3:2 (*29*).
31. H. F. Levison, S. A. Stern, *Icarus* **116**, 315 (1995).
32. J. Hahn, W. R. Ward, *Lunar Planet. Sci. Conf.* **XXVI**, 541 (1995).
33. A. R. Dobrovolskis, S. J. Peale, A. W. Harris, in *Pluto and Charon*, S. A. Stern, D. J. Tholen, Eds. (Univ. Arizona Press, Tucson, 1997), pp. 159–190.
34. R. Malhotra, *Astron. J.* **110**, 420 (1995).
35. S. Sridhar, S. Tremaine, *Icarus* **95**, 86 (1992).
36. H. A. Williams, J. E. Tohline, *Astrophys. J.* **334**, 449 (1988).
37. This research was supported by the NSF under grant no. AST0307933. J. Melosh and B. Pierazzo are gratefully acknowledged for providing the M-ANEOS equation of state and related material constants. This paper has benefited from previous work and discussions with E. Asphaug, W. Ward, A. Stern, R. Mihran, B. McKinnon, S. Kenyon, and H. Levison and from two anonymous and helpful reviews. A. Stern, L. Young, C. Olkin, and B. Bottke provided helpful comments on the manuscript, and Southwest Research Institute provided the computational resources.

Farming and the Fate of Wild Nature

Rhys E. Green,[1,2]* **Stephen J. Cornell,**[1,3] **Jörn P. W. Scharlemann,**[1,2] **Andrew Balmford**[1,4]

World food demand is expected to more than double by 2050. Decisions about how to meet this challenge will have profound effects on wild species and habitats. We show that farming is already the greatest extinction threat to birds (the best known taxon), and its adverse impacts look set to increase, especially in developing countries. Two competing solutions have been proposed: wildlife-friendly farming (which boosts densities of wild populations on farmland but may decrease agricultural yields) and land sparing (which minimizes demand for farmland by increasing yield). We present a model that identifies how to resolve the trade-off between these approaches. This shows that the best type of farming for species persistence depends on the demand for agricultural products and on how the population densities of different species on farmland change with agricultural yield. Empirical data on such density-yield functions are sparse, but evidence from a range of taxa in developing countries suggests that high-yield farming may allow more species to persist.

Clearance for cropland or permanent pasture has already reduced the extent of natural habitats on agriculturally usable land by more than 50% (*1–3*), and much of the rest has been altered by temporary grazing (*4*).

Intensive management to increase production—through irrigation and the application of fertilizers and pesticides—can further reduce the wildlife value of farmed land. Although growth in global food production outstripped population growth between 1961 and 1999, this was achieved through a 12% increase in the global area of cropland and a 10% rise in the area of permanent pasture (*2, 3*). Overall food crop yield per unit area (*3*) grew by 106%, but this was linked to a 97% rise in the area of land under irrigation, and 638%, 203%, and 854% increases, respectively, in the use of nitrogenous and phosphate fertilizers and the production of pesticides (*2, 5, 6*). These impacts look set to grow still further (*5*). With the human population predicted to rise to between 8 and 10 billion (*7, 8*) and with rapidly increasing per capita consumption (*9*), overall food demand is expected to increase two- to threefold by 2050 (*6, 10*). Here, we propose an agenda for the research needed to identify how this enormously increased demand can be met at the least cost to the other species with which we share our planet.

Agricultural change: A tale of two worlds. From the perspectives of both development and conservation, globally averaged changes in agriculture mask important spatial variation, with more pronounced recent changes in the developing world, where most species reside. For instance, since 1961 the total area of cropland in the developing world has increased by over